RSC Advances

ROYAL SOCIETY OF CHEMISTRY

www.rsc.org/advances

Graphical abstract

Ni-enhanced Co_3O_4 nanoarrays in-situ grown on Cu substrate as integrated anode materials for high-performance Li-ion batteries

Xiaoyu Liu，Shimou Chen，Jia Yu，Wenlong Zhang，Yajie Dai[a], Suojiang Zhang[b]

3D Co_3O_4 nanoarrays fabricated on the Cu substrate surface with a Ni-nanoseed-layer as interface was synthesized by a two-step approach, combing electrodeposition and hydrothermal synthesis. The Ni-nanoseed-layer improved the mechanical adhesion between nanoarrays and substrates without binders, while increasing the conductivity of anodes without conductive additives. This integrated anode exhibited excellent performance in Li-ion batteries.

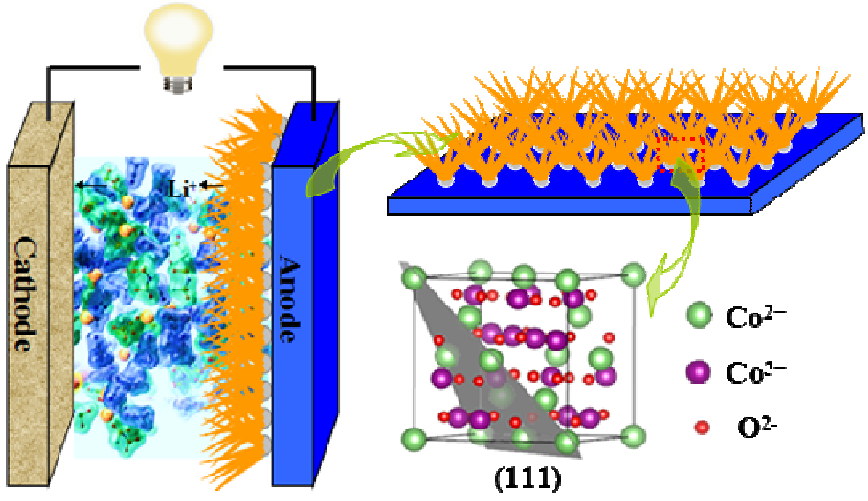

RSC Advances

RSCPublishing

PAPER

Ni-enhanced Co_3O_4 nanoarrays in-situ grown on Cu substrate as integrated anode materials for high-performance Li-ion batteries

Cite this: DOI: 10.1039/x0xx00000x

Received 00th,
Accepted 00th

DOI: 10.1039/x0xx00000x

www.rsc.org/

Xiaoyu Liu,[‡ab] Shimou Chen,[‡b] Jia Yu,[b] Wenlong Zhang,[a] Yajie Dai[*a] and Suojiang Zhang[*b]

A two-step strategic approach was proposed to synthesize three-dimensional Co_3O_4 nanoarrays fabricated on the Cu substrate surface with a Ni layer as interface. Firstly, a Ni-nanoseed-layer was prepared on a Cu substrate by electrodepositing Ni. And then Co_3O_4 nanoarrays were in-situ grown on the Ni layer via a hydrothermal synthesis. The as-obtained materials were directly used as anodes for Li-ion batteries, the electrodes maintained a high capacity up to 1150 mAh/g at 0.1C after 30 cycles, and showed an excellent cycling stability and rate capability. The good electrochemical performance was owed to the pre-electrodeposited Ni-nanoseed-layer, because the Ni layer could improve the mechanical adhesion between Co_3O_4 nanoarrays and substrates effectively and increase the conductivity of anodes, without applying binders or conductive additives. This strategic in-situ synthesis method will probably open a new avenue for the development of integrated electrode materials for high-performance Li-ion batteries.

Introduction

Along with the rapid development of economy and society, new energy-materials are extensively used in many areas, including portable electronics, electric vehicles, and smart grids.[1-4] Therefore researches on battery materials with high capacity, cycling stability and security are necessary. As the Li-ion battery (LIB) has many advantages including high energy density, large output power, and being friendly to the environment, it plays an irreplaceable role in the secondary energy supply.[5-8] Transition-metal oxide materials such as cobalt oxide and nickel oxide are promising high-energy-density anode materials. Among them cobalt-based electrode materials are attractive due to their high electrochemical activity and ease of processing,[9] and Co_3O_4 as anode material has attracted more interest owing to its superior specific capacity (896mAh/g in theory),[10-13] which is much higher than that of commercial graphite anode (~372mAh/g). However, relatively poor capacity retention upon cycling and low rate capability of Co_3O_4 restrict its practical application in LIBs as a high-performance anode. Different approaches have been utilized to improve the electrochemical properties of Co_3O_4, such as the use of Co_3O_4/carbon nanocomposites, nanoscale Co_3O_4 and mesoporous Co_3O_4. In addition to the above approaches, considerable effort has been devoted to develop Co_3O_4 materials with three-dimensional (3D) microstructure,[14] since the unique morphology can significantly enhance electrochemical performance: 1) The 3D microstructure provide better access for Li ions due to a larger electrode/electrolyte interface, and shorter diffusion paths for Li ions and electrons, leading to improved rate capability.[15,16] 2) The free space among nanoarrays can effectively buffer the large volume change during Li insertion/extraction, thus contribute to better cycling stability.[17,18] 3) The 3D nanoarrays show stable structural support and multiple interconnections across nanowires.

Besides the 3D nanoarray microstructure, we inferred that if Co_3O_4 nanoarrays could be in-situ grown on the current collector while maintaining a good contact, it would show better cycling performance and durability when used as LIB anode materials directly. Considering the low-cost Cu sheets are common current collecting substrates, we proposed that 3D Co_3O_4 nanoarrays fabricated on Cu substrates are promising anode materials, since this integrated anode can enhance electrical conductivity and enlarge reaction surface.[19-21] However, free-standing Co_3O_4 nanoarrays grown directly on Cu sheets have rarely been realized.[22] As the adhesion between nanoarrays and Cu substrates is weak, active

[a] *School of Electrical and Electronic Engineering, Harbin University of Science and Technology, Harbin, Heilongjiang,150040，PR China. E-mail: yajiedai@yeah.net*

[b] *Beijing Key Laboratory of Ionic Liquids Clean Process, Key Laboratory of Green Process and Engineering, Institute of Process Engineering (IPE), Chinese Academy of Sciences (CAS), Beijing 100190, PR China. E-mail: sjzhang@home.ipe.ac.cn*

† Electronic Supplementary Information (ESI) available: Experimental part, EDS mapping, SEM images and Cycling performance. See DOI: 10.1039/c000000x/

‡These authors contributed equally to this work.

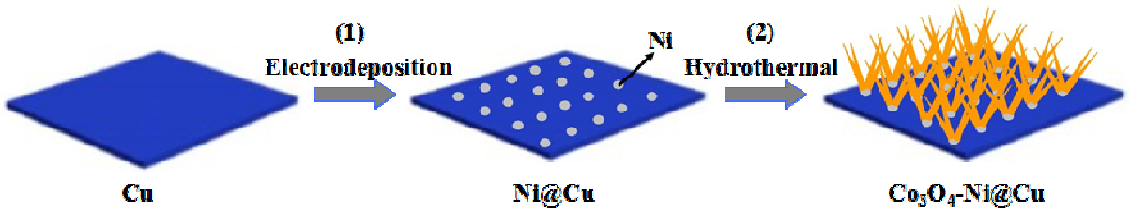

Figure 1 Schematic for the growth process of Co_3O_4-Ni@Cu (two-step method).

materials are easy to fall off during the charging/discharging process, thus greatly reduces the cycling stability and energy density.

In this paper, we successfully prepared Ni-enhanced Co_3O_4 nanoarrays in-situ grown on Cu substrate as integrated anode for high-performance LIBs, by a two-step approach. The new synthetic strategy combined two synthesis methods of electrodeposition of Ni-nanoseed-layer and hydrothermal synthesis. We found that pre-electrodepositing Ni-nanoseed-layer onto the Cu substrate could improve the mechanical adhesion between Co_3O_4 nanoarrays and substrates effectively and increase the conductivity of anodes, without applying binders or conductive additives. Those were the principal reasons for improved performance. In addition, we preliminarily speculated that the Ni layer might play some role in influencing the growth of Co_3O_4 nanoarrays, promoting the formation of nanoarrays with dominant (111) crystal planes that show much better performance than (001) planes.[23] Finally, when as-obtained Ni-enhanced Co_3O_4 nanoarrays were investigated as anode materials for LIBs, these integrated electrodes indeed exhibited good specific capacity, cycling stability and rate capability.

Experimental

Electrodeposition of Ni Nanoseeds.

Firstly, we carefully cleaned the Cu sheet in mixed acid solution for 5 min in order to remove the surface CuO layer, and then used deionized water and ethanol in turn to wash, repeating several times. Subsequently we electrodeposited Ni nanoparticles onto the Cu substrate (1×3 cm^2 in size). The concentration of plating solution was 250g/L $NiSO_4 \cdot 6H_2O$, 30g/L $NiCl_2 \cdot 6HO$, 35g/L H_3BO_3 and 0.1g/L sodium dodecyl sulfate (SDS), while the pH value was set at 3~5. In the three-electrode electrochemical cell, the acid-treated Cu worked as working electrode, Ni plate worked as counter electrode and reference electrode. Electrodepositing Ni was carried out at 45℃ with a stirring speed of 700 r/min, by imposing a constant current. The Ni depositing time was 60s.

Synthesis of Co_3O_4 nanoarrays.

Co_3O_4 nanoarrays were prepared by a hydrothermal synthesis method. Firstly, 1.46g of $Co(NO_3)_2$ $6H_2O$, 0.37g of NH_4F and 1.5g of $CO(NH_2)_2$ were dissolved in 50 mL of distilled water. After being stirring slightly for 40min, the solution was transferred into Teflon-lined stainless steel autoclave. The Cu substrate coated by Ni-nanoseed-layer was immersed into the reaction solution with a tilt angle of 45 degree. The stainless steel autoclave was sealed and heated at 120 ℃ for 5 h, and then the autoclave was cooled down to room temperature. After the reaction, the samples were rinsed with distilled water for several times. Finally, the Ni-enhanced Co_3O_4 nanoarrays in-situ grown on Cu substrate was obtained after annealing the samples at 450 ℃ in air for 3h, with a color changing of the samples from pink to black.

Characterization

The X-ray diffraction (XRD) patterns were recorded on a Bruker D8 Focus X-ray diffractometer with Ni-filtered Cu-Kα radiation (λ = 0.15406 nm). The scanned 2θ range was between 40° and 95° at room temperature. X-ray photoelectron spectroscopy (XPS, PHI 5700),scanning electron microscopy(SEM,JEOL JSM-7001F) and high-resolution transmission electron microscopy(JEOL JEM-2100).

Electrochemical measurements

Simulation of the battery were directly fabricated from the Co_3O_4-Ni@Cu as the working electrode without any ancillary materials.The electrolyte used was $LiPF_6$ (1M) /EC+DEC+DMC (1:1:1, weight).The galvanostatic charge/discharge tests were performed using LAND battery testing system in the voltage range of 0.01-3.2 V at room temperature.

Results and discussion

Figure 1 shows the two-step synthesis strategy for the Co_3O_4 nanoarrays by the combination of electrodeposition and hydrothermal synthesis. Firstly, Ni nanoparticles were electrodeposited onto the Cu substrate as seeds.[24] this sample was named Ni@Cu for simplicity. Subsequently Co_3O_4 nanoarrays were in-situ grown upwards from the Ni-nanoseed-layer on the Cu substrate directly, using hydrothermal synthesis, followed by a calcinations treatment. Impressively, the synthesized integrated anode material showed a high specific capacity, an excellent rate capacity and a good cycling stability.

The as-obtained final products of Ni-enhanced Co_3O_4 nanoarrays were named Co_3O_4-Ni@Cu for simplicity. The Energy-dispersive X-ray spectrometry (EDS) mapping analysis shown in Figure S1 (ESI) proves the existence of the Co_3O_4-Ni@Cu. The corresponding XRD patterns of Ni@Cu samples are provided in Figure 2. Figure 2a and 2b show the XRD pattern of the Cu substrates after being electrodeposited with Ni layer for 60s and 200s, respectively. It was found that the Ni peak was not obvious in a relatively short electrodepositing time, almost all peaks in Figure 2a belonging to Cu (Figure 2a). However, when the Ni electrodepositing time reached 200s, Ni peaks could be observed clearly in Figure 2b, indicating that the Ni-seed-layer was successfully deposited on the surface of Cu substrate.[25,26] Moreover, as shown in Figure S2 (ESI), the presence of Co_3O_4, Ni and Cu in Co_3O_4-Ni@Cu was proved by XRD spectrum.

In order to clarify the components of the final product of Ni-enhanced Co_3O_4 nanoarrays and find some clues about the growth

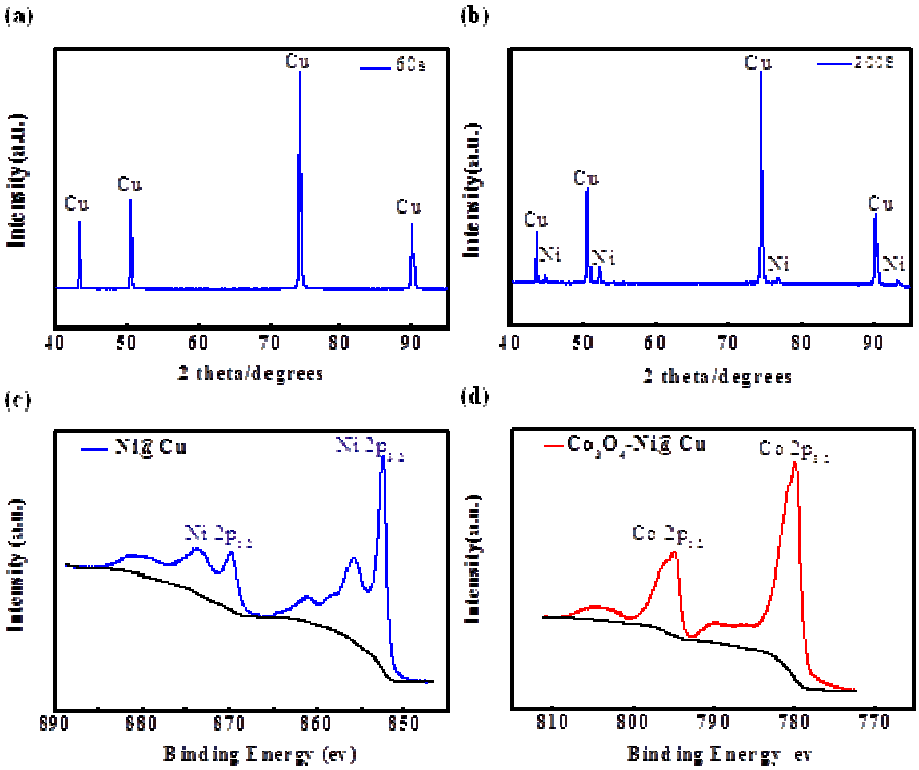

Figure 2 (a) (b) XRD patterns of the products after being electrodeposited with Ni, while the electrodepositing time was 60s and 200s, respectively. (c) XPS peaks of Ni2p of the Cu substrate after being electrodeposited with Ni (Ni@Cu) and (d) XPS peaks of Co2p of the final product (Co_3O_4-Ni@Cu).

mechanism, the Ni@Cu and Co_3O_4-Ni@Cu samples were characterized by XPS. As shown in Figure 2c, the Ni@Cu sample showed $Ni2p_{3/2}$ and $Ni2p_{1/2}$ peaks which are centered at 852.6 and 873.85 eV, respectively, confirming that the elementary Ni was deposited on the surface of Cu substrates. We suggested that Co_3O_4 nanoarrays were in-situ grown from the Ni-nanoseed-layer which was firstly electrodeposited onto Cu substrate. Ni nanoseeds formed a connection layer between the Co_3O_4 nanoarrays and Cu substrate, playing a key role in stabilizing the nanoarrays grown on Cu substrates. In addition, as seen in Figure 2d, the Co_3O_4-Ni@Cu sample exhibited peaks of $Co2p_{1/2}$ and $Co2p_{3/2}$ at 795.2 eV and 780.2 eV,[8] respectively. The XRD and XPS results indicated that the final product was Ni-enhanced Co_3O_4 composite.

The morphology of Ni-nanoseed-layer on Cu substrate (Ni@Cu) was shown in Figure 3a, we observed that the Ni nanoseeds were successfully growth on the Cu substrate. Similarly, Figure 3b displayed the SEM photograph of 3D Co_3O_4-Ni@Cu composite nanoarrays, which were electrodeposited with Ni for 60s and hydrothermal treated at 120 ℃ for 5h. The as-obtained Ni-enhanced Co_3O_4 nanowires had an average diameter of 100nm. In addition, various steps of formation of layers were proved by color changing (as seen in inset), from silver (Ni@Cu) to black (Co_3O_4-Ni@Cu).[27] In contrast, Figure S3 (ESI) displayed the SEM images of Co_3O_4@Cu nanoarrays without Ni nanoseeds. Moreover, too short or too long electrodepositing time was not favorable for the formation of Co_3O_4-Ni@Cu composite nanoarrays. As shown in Figure S4 (ESI), when the electrodepositing time was only 2s, we observed that the Co_3O_4 nanoarrays were sparser than those with an electrodepositing time of 60s. By contrast, when the electrodepositing time increased to 6000s, the anode materials were likely to crack, and Co_3O_4 active materials were inclined to fall from the Ni-nanoseed-layer.

Further structural characterizations of the Ni-enhanced Co_3O_4 nanoarrays and Co_3O_4 nanoarrays without Ni were performed by TEM, as shown in Figure 4a and 4c. Obviously, plenty of pores were

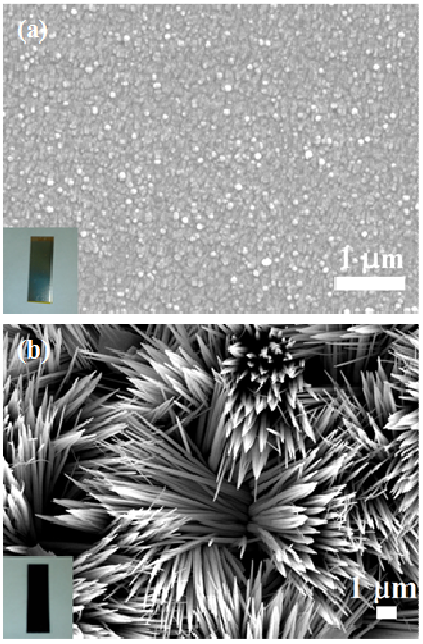

Figure 3 (a) Low-magnification SEM images of Ni@Cu, the Ni electrodepositing time is 60s (b)SEM images of the Co_3O_4-Ni@Cu nanoarrays, the hydrothermal synthesis condition: 120 ℃ for 5h. Inset: photographs of the products in different reaction steps.

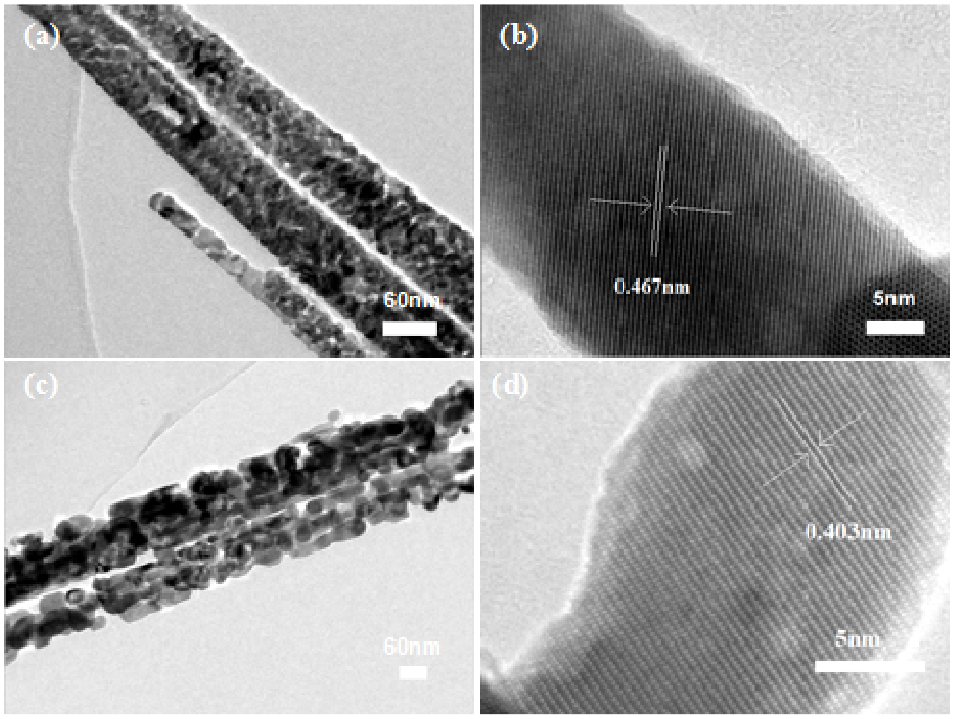

Figure 4 (a) TEM image of Co_3O_4 nanoarrays in-situ grown on Cu substrates with Ni-nanoseed-layer. (b) HRTEM image of the above Co_3O_4 nanoarrays, showing a dominant (111) crystal plane. (c) TEM image of Co_3O_4 nanoarrays grown on Cu substrates directly without Ni-nanoseed-layer. (d) HRTEM image of the above Co_3O_4 nanoarrays, showing a dominant (001) crystal plane.

distributed uniformly on the nanoarray surface due to the gas-releasing (CO_2, H_2O) during the calcination process,[28,29] which can provide a quite short diffusion path for Li ions and electrons when used as anode materials for LIBs.[30-32] In Figure 4b which was taken from Co_3O_4 nanoarrays in-situ grown on Cu substrates with Ni-nanoseed-layer, we found that a measured interplanar spacing of 0.467 nm was in good agreement with the spacing of the Co_3O_4 (111) planes.[22] In Figure 4d which was taken from Co_3O_4 nanoarrays grown on Cu substrates directly without Ni-nanoseed-layer, it showed a measured interplanar spacing of 0.403 nm which was in good agreement with the spacing of the Co_3O_4 (001) planes. In general, for HRTEM results we found that Ni-enhanced Co_3O_4 nanoarrays had dominant (111) crystal planes while Co_3O_4 nanoarrays without Ni-nanoseed-layer showed dominant (001) crystal planes. Moreover, in previous work, addition of seed layer in nanostructure synthesis had been found to change the growth orientation and morphologies of nanostructure, such as ZnO, TiO_2 and SnO_2 nanomaterials.[33-36] Based on these work related to seed-layer and HRTEM results, here we preliminarily inferred that the Ni-nanoseed-layer might play some role in influencing the growth of Co_3O_4 nanoarrays and promote the formation of Co_3O_4 nanoarrays with (111) crystal planes. The relationship of Ni-nanoseed-layer and Co_3O_4 nanoarray crystal plane will be studied in future research.

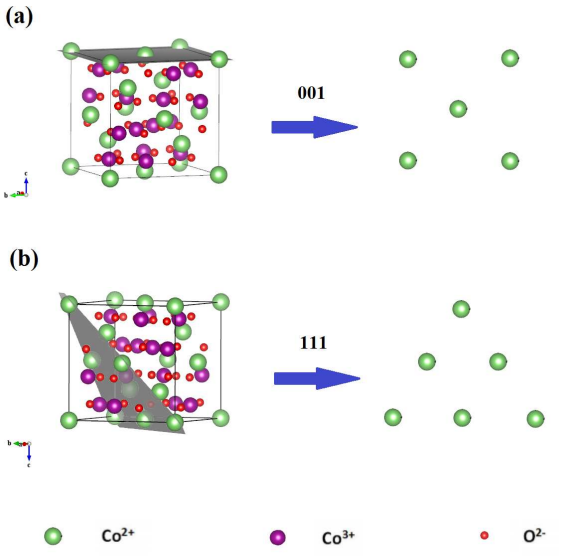

Figure 5 Theoretical models of various crystal planes of Co_3O_4. The 3 D and 2 D surface atomic configurations of (a) (001) plane and (b) (111) plane of Co_3O_4.

Recently, nanostructures exposing highly reactive crystal planes begin to exhibit great potentials for electrochemical energy storage. Li et al systematically summarized the relationship between crystal plane of Co_3O_4 and electrochemical performance, and observed that Co_3O_4 nanoparticles with (111) planes showed better cycling and rate performances than those with (001) planes.[23] To further illustrate, the atomic configurations for various crystal planes of the Co_3O_4 unit cell are shown in Figure 5. As shown in Figures 5a and b, the (001) plane contains only 2 Co^{2+} while the (111) plane has 3.75 Co^{2+}, showing that the (111) crystal plane has more Co^{2+} than the (001) plane. According to the charge/discharge mechanism of Co_3O_4,[37-39] (111) crystal planes have a faster Co^{2+} /Co^0 redox reaction, which brings better electrochemical performance such as higher rate capability. Therefore, we could predict that Co_3O_4 nanoarrays with dominant (111) crystal planes would exhibit better electrochemical performance than those with dominant (001) crystal planes.

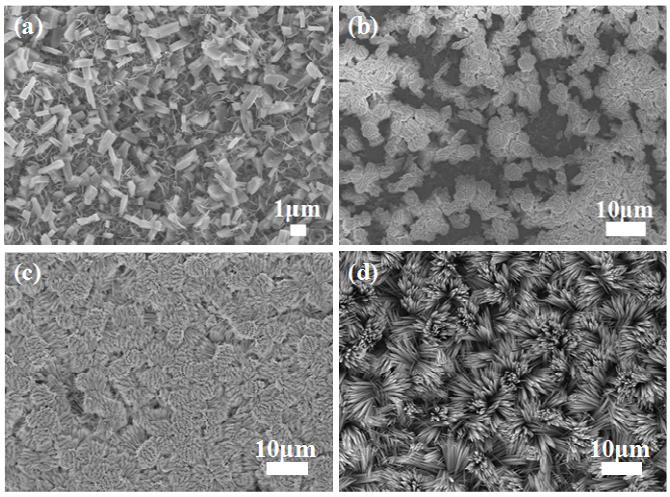

Figure 6 SEM images of Co_3O_4-Ni@Cu precursors synthesized at 463 K for different time: a) 20min, b) 40min, c) 1h and d) 5h.

Formation process of the 3D Co_3O_4-Ni@Cu products was further investigated for different reaction stages, Fig. 6a-d are the SEM images of products obtained at different hydrothermal reaction times. When the hydrothermal treatment time was 20 min, we observed that lots of Co_3O_4 nanorods formed on the Cu substrate surface, as shown in Figure 6a. However, when the reaction time reached 40 min, non-uniform clusters of nanowires formed initially. After reacting for 1h, the Cu substrate was completely covered by the fast-growing Co_3O_4 nanoarrays. We obtained the final product after 5 h of hydrothermal treatment (Figure 6d).

To further investigate the role of Ni-nanoseed-layer in the Co_3O_4 nanoarrays in-situ grown on Cu substrates, we did a controlled experiment, in which we fabricated Co_3O_4 nanoarrays directly grown on the Cu substrates, without pre-depositing Ni-nanoseed-layer on Cu. The anode performance of the Co_3O_4-Ni@Cu nanoarrays as well as the Co_3O_4@Cu for LIBs was both evaluated, with the standard Co_3O_4@Cu/Li and Co_3O_4-Ni@Cu/Li half-cell configurations. The first three charging–discharging voltage profiles of Co_3O_4@Cu and Co_3O_4-Ni@Cu samples were shown in Figure 7a and 7b, respectively, with a current rate of 0.1 C and a voltage range of 0.01–3.2V (versus Li/Li^+). In the first-discharge curves, both of them exhibit voltage plateaus at 1.25 V, subsequently declines to cutoff voltages of 0.05 V gradually, indicating typical characteristics of voltage profiles trends for Co_3O_4 anode. The Co_3O_4@Cu anode exhibited initial charge and discharge capacities of 1000 mAh/g and 1365 mAh/g, respectively, while the coulombic efficiency was 73%. Meanwhile, the Co_3O_4-Ni@Cu anode had higher charge and discharge capacities of 1300 mAh/g and 1816 mAh/g, respectively, with a coulombic efficiency of 71%. The first discharge capacities of the two anodes were higher than the theoretical capacity (890 mAh/g). The difference can be attributed to the formation of a solid electrolyte interface (SEI) layer and possibly interfacial lithium storage.[40-42] Obviously, the Co_3O_4-Ni@Cu anode show a much higher first discharge capacity than that of Co_3O_4@Cu. Therefore, electrodeposition Ni nanoseeds is suggested to be an effective technique to improve the specific capacity of Co_3O_4 nanoarrays anodes.

Figure 7c compares the cycling performance of Co_3O_4@Cu and Co_3O_4-Ni@Cu anode materials with a high current rate of 1 C. The Co_3O_4-Ni@Cu anode exhibited little capacity fading after 100 cycles, maintaining a discharge capacity of 610 mAh/g and a coulomb efficiency of 100%. By contrast, the Co_3O_4@Cu anode showed a discharge capacity of only 200 mAh/g after 100 cycles. The discharge capacity of Co_3O_4-Ni@Cu nanoarrays anode was almost triple that of Co_3O_4@Cu anode. Moreover, Figure S5 (ESI) highlighted that the Co_3O_4-Ni@Cu nanoarrays anode maintained a quite high specific capacity as high as 1150 mAh/g after 30 cycles, with a current rate of 0.1 C. The better cycling performance of

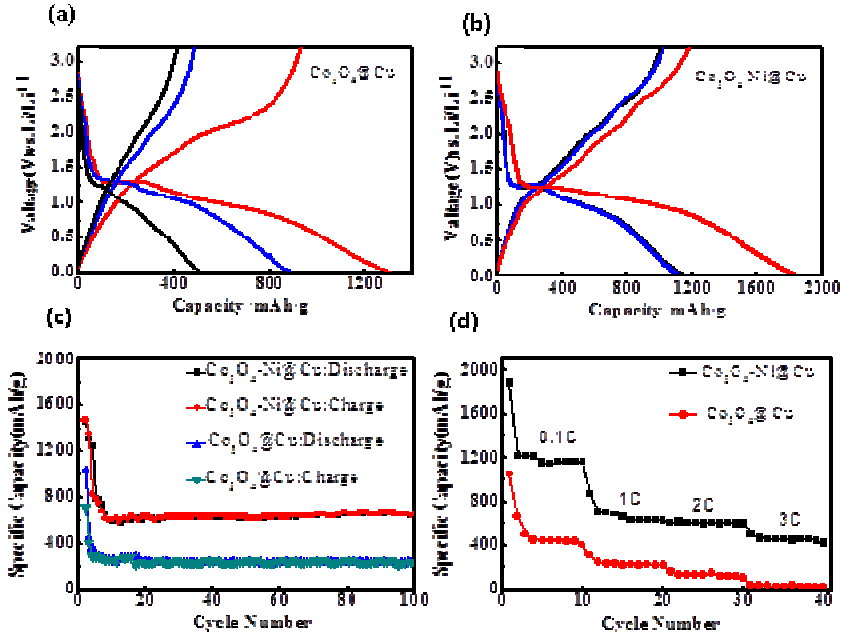

Figure 7 (a), (b) First three charging–discharging curves for Co_3O_4@Cu and Co_3O_4-Ni@Cu nanoarray anodes, respectively, with a voltage range of 0.01–3.2 V and a current of 0.1 C. (c) Cycling performance of the Co_3O_4@Cu and Co_3O_4-Ni@Cu nanoarray anodes with a current of 1C. (d) Discharging curves for Co_3O_4@Cu and Co_3O_4-Ni@Cu nanoarray anodes at different rates.

Co_3O_4-Ni@Cu anode was suggested to be mainly owed to the pre-electrodepositing Ni-nanoseed-layer which improved the mechanical adhesion between Co_3O_4 nanoarrays and substrates effectively.

As the rate capability is quite critical for practical applications of LIBs, discharge curves at various current densities for the Co_3O_4-Ni@Cu and Co_3O_4@Cu anodes were shown in Figure 7d. The charge/discharge capacities with different rates (0.1C, 1C, 2C, and3C, 1 C = 890 mA/g) were investigated while each rate was measured 10 times. When compared with Co_3O_4@Cu, the Co_3O_4-Ni@Cu nanoarrays anode showed a much better rate capability. More specifically, Co_3O_4-Ni@Cu anode showed discharge capacities of 1043 mAh/g, 651 mAh/g, 595 mAh/g and 502 mAh/g with rates of 0.1, 1, 2 and 3C, respectively. It was found that Co_3O_4-Ni@Cu showed only a little capacity fading when the discharge rate increased from 1 C to 3 C. By contrast, without pre-electrodepositing Ni-nanoseed-layer, the Co_3O_4@Cu only maintained discharge capacities of 446 mAh/g, 227 mAh/g, 125 mAh/g and 26 mAh /g with rates of 0.1, 1, 2 and 3C, respectively. The improved rate capability of Co_3O_4-Ni@Cu nanoarrays anode was suggested to be ascribed to the increased conductivity of anodes, as well as the improved mechanical adhesion between Co_3O_4 nanoarrays and substrates due to the Ni-nanoseed-layer.

Figure S6 (ESI) showed the impedance of Co_3O_4-Ni@Cu and Co_3O_4@Cu nanoarray anodes. Both of the impedance spectra had similar characteristics: a depressed semicircle at the high-medium frequency as well as an inclined line at the low frequency which were in good agreement with previously reported impedance spectra of Co_3O_4.[43] The inclined lines were ascribed to the lithium diffusion impedance. And the depressed semicircles were attributed to charge impedance.[44] It indicated that the Co_3O_4-Ni@Cu structure helped improve the conductivity of the anode, when compared with Co_3O_4@Cu anode without Ni-nanoseed-layer. In addition, as shown in Figure 8, the nanoarrays microstructure of Co_3O_4-Ni@Cu was well preserved after 10 cycles and 30 cycles with a current of 1 C, even after 100 cycles, the skeleton of the Co_3O_4 nanoarrays still maintained (Figure 8e and 8f), revealing an excellent structural stability during charge-discharge cycles.

In this study, the integrated anode composed of Ni-enhanced Co_3O_4 nanoarrays in-situ grown on Cu substrate exhibited far better electrochemical performance than those made of Co_3O_4 nanoarrays without Ni-nanoseed-layer. The excellent properties should be owed to several factors: First, Ni-nanoseed-layer improved the mechanical adhesion between Co_3O_4 nanoarrays and Cu substrates effectively, thus enhanced the cycling stability. Second, the Co_3O_4-Ni@Cu system increased the conductivity of anode materials. Third, the 3D Co_3O_4 nanoarrays microstructure provided larger electrode/electrolyte interface, shorter diffusion paths and larger free volume, contributing to better electrochemical performance as anode material for LIBs. Forth, we preliminarily inferred that the Ni layer might play some role in influencing the growth of Co_3O_4 nanoarrays and led to dominant (111) crystal planes, which exhibited better performance than (001) planes. It appears promising to further enhance the electrochemical properties of Co_3O_4 integrated anodes through improving their crystal plane structure and introducing nanoseed layers.

Conclusion

In summary, we demonstrated a facile synthesis method of Co_3O_4 nanoarrays in-situ grown on Cu substrates directly, by a combination of pre-electrodepositing Ni-nanoseed-layer and controlled hydrothermal synthesis. The as-prepared Co_3O_4-Ni@Cu nanoarrays electrode exhibited excellent electrochemical performance as anode materials for LIBs: They showed a quite high charge/discharge capacity of ~1150 mAh/g with a current of 0.1C, while exhibited good cycling stability and rate capability. The high electrochemical performance was owed to the unique feature of the as-obtained Ni-enhanced Co_3O_4 nanoarrays: Besides the larger electrode/electrolyte interface, shorter diffusion paths and larger free volume due to the nanoarrays microstructure, the Ni-nanoseed-layer pre-electrodeposited on the Cu substrate could improve the mechanical adhesion between Co_3O_4 nanoarrays and substrates and enhance the conductivity of anodes, without applying binders or conductive additives. Given their facile in-situ synthesis and improved performance, this work will open a new avenue for the development of integrated electrode materials for high-performance LIBs.

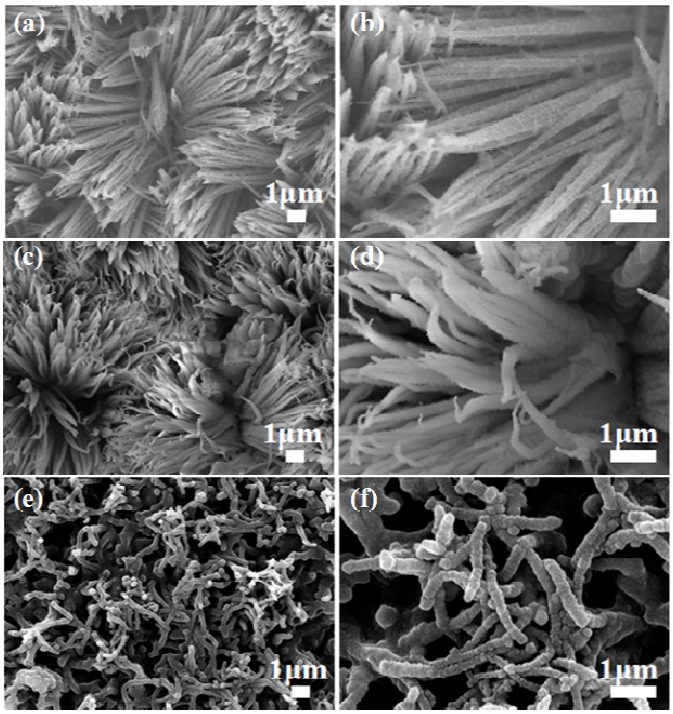

Figure 8 (a,b) (c,d) (e,f) The SEM images of the Co_3O_4-Ni@Cu nanoarrays tested as LIBs anode after 10, 30 and 100 cycles, respectively.

Acknowledgement

† This work was supported by National Natural Science Foundation of China (No. 21276257) and Beijing Natural Science Foundation (2132054) and "Strategic Priority Research Program" of the Chinese Academy of Sciences (Grant No. XDA09010103）

References

1 Y. Gogotsi and P. Simon, *Science*, 2011, **334**, 917-918.
2 Y. F. Deng, Z. E. Li, Z. C. Shi, H. Xu, F. Peng and G. H. Chen, *RSC Adv.*, 2012, **2**, 4645–4647.
3 H. B. Wu, J. S. Chen, H. H. Hng and X. W. Lou, *Nanoscale*, 2012, **4**, 2526-2542.

4 J. B. Goodenough and Y. Kim, *Chem. Mater.*, 2010, **22**, 587-603.
5 J. Liu, Y. C. Zhou, F. Liu, C. P. Liu, J. B. Wang, Y. Pan and D. F. Xue, *RSC Adv.*, 2012, **2**, 2262–2265.
6 B. Dunn, H. Kamath and J. M. Tarascon, *Science*, 2011, **334**, 928-935.
7 X. M. Liu, Q. Long, C. H. Jiang, B. B. Zhan, C. Li, S. J. Liu, Q. Zhao, W. Huang and X. C. Dong, *Nanoscale*, 2013, **5**, 6525-6529.
8 J. Y. Wang, N. L. Yang, H. J. Tang, Z. H. Dong, Q. Jin, M. Yang, D. Kisailus, H. J. Zhao, Z. Y. Tang and D. Wang, *Angew. Chem. Int. Ed.*, 2013, **52**, 6417-6420.
9 Y. Qi, H. Zhang, N. Du, C. X. Zhai and D. Yang, *RSC Adv.*, 2012, **2**, 9511-9516.
10 L. Li, K. H. Seng, Z. X. Chen, Z. P. Guo and H. K. Liu, *Nanoscale*, 2013, **5**, 1922–1928.
11 X. H. Xia, J. P. Tu, Y. Q. Zhang, Y. J. Mai, X. L. Wang, C. D. Gu and X. B. Zhao, *RSC Adv.*, 2012, **2**, 1835–1841.
12 M. Okubo, E. Hosono, T. Kudo, H. S. Zhou and I. Honma, *Solid State Ionics*, 2009, **180**, 612–615.
13 R. H. Wang, C. H. Xu, J. Sun, Y. Q. Liu, L. Gao and C. C. Lin, *Nanoscale*, 2013, **5**, 6960-6967.
14 H. B. Wu, J. S. Chen, H. H. Hng and X. W. Lou, *Nanoscale*, 2012, **4**, 2526-2542.
15 X. H. Xia, J. P. Tu, Y. Q. Zhang, J. Chen, Xi. L.Wang, C. D. Gu, C. Guan, J. S. Luo and H. J. Fan, *Chem. Mater.*, 2012, **24**, 3793–3799.
16 B. G. Choi, S. J. Chang, Y. B. Lee, J. S. Bae, H. J. Kim and Y. S. Huh, *Nanoscale*, 2012, **4**, 5924-5930.
17 W. J. Hao, S. M. Chen, Y. J. Cai, L. Zhang, Z. X. Li and S. J. Zhang, *J. Mater. Chem. A*, 2014, **2**, 13801-13804.
18 W. Wang, M. Tian, A. Abdulagatov, S. M. George, Y. C. Lee and R. G. Yang, *Nano Lett.*, 2012, **12**, 655–660.
19 Q. Yang, Z. Y. Lu, Z. Chang, W. Zhu, J. Q. Sun, J. F. Liu, X. M. Sun and X. Duan, *RSC Adv.*, 2012, **2**, 1663–1668.
20 Y. Gao, S. Chen, D. Cao, G. Wang and J. Yin, *J. Power Sources*, 2010, **195**, 1757–1760.
21 J. Jiang, J. P. Liu, R. M. Ding, X. X. Ji, Y. Y. Hu, X. Li, A. Z. Hu, F. Wu, Z. H. Zhu and X. T. Huang, *J. Phys. Chem. C*, 2010, **114**, 929-932.
22 X. Y. Xue, S.Yuan, L. L. Xing, Z. H. Chen, B. He and Y. J. Chen, *Chem. Commun.*, 2011, **47**, 4718-4720
23 X. L. Xiao, X. L. Liu, H. Zhao, D. F. Chen, F. Z. Liu, J. H Xiang, Z. B. Hu and Y. D. Li, *Adv. Mater.*, 2012, **24**, 5762–5766.
24 R. P. Silva, S. Eugénio, T. M. Silva, M.J. Carmezim and M. F. Montemor, *J. Phys. Chem.C*, 2012, **116**, 22425–22431.
25 J. Y. Liao, D. Higgins, G. Lui, V. Chabot, X. C. Xiao and Z. W. Chen, *Nano Lett.*, 2013, **13**, 5467–5473.
26 B. X. Li, Y. Xie, C. Z. Wu, Z. Q. Li and J. Zhang, *Mater. Chem. Phys.*, 2006, **99**, 479-486.
27 R. Xu and H. C. Zeng, *J. Phys. Chem. B*, 2003, **107**, 12643-12649.
28 L. Q. Mai, F. Dong, X. Xu, Y. Z. Luo, Q. Y. An, Y. L. Zhao, J. Pan and J. N. Yang, *Nano Lett.*, 2013, **13**, 740–745.
29 Y. J. Feng, R. Q. Zou, D. G. Xia, L. L. Liu and X. D. Wang, *J. Mater. Chem. A*, 2013, **1**, 9654-9658.
30 S. R.Gowda, A. L. M. Reddy, M. M. Shaijumon, X. B. Zhan, L. J. Ci and P. M. Ajayan, *Nano Lett.*, 2011, **11**, 101-106.
31 C. K. Chan, H. L. Peng, G. Liu, K. McIlwrath, X. F. Zhang, R. A. Huggins and Y. Cui, *Nat. Nanotechnol.*, 2008, **3**, 31-35.
32 F. Zhan, B. Geng and Y. Guo, *Chem. Eur. J.*, 2009, **15**, 6169-6174.
33 M. Y. Liao, L. Fang, C. L. Xu, F. Wu, Q. L. Huang and M. Saleem, *Mat. Sci. Semicon. Proc.*, 2014, **24**, 1-8.
34 Z. F. Liu, J. Ya and L. E, *J. Solid. State. Elect.*, 2010, **14**, 957-963.
35 Y. F. Wang, B. X. Lei, Y. F. Hou, W. X. Zhao, C. L. Liang, C. Y. Su and D. B. Kuang, *Inorg. Chem.*, 2010, **49**, 1679-1686.
36 Z.H. Ibupoto, K. Khun, J. Lu, X. J. Liu, M. S. AlSalhi, M. Atif, A. A. Ansari and M. Willander, *J. Cryst. Growth*, 2013, **368**, 39-46.
37 M. V. Reddy , Z. Beichen , L. J. Nicholette , K. M. Zhang and B. V. R. Chowdari , Electrochem. *Solid State Lett.*, 2011, **14** , A79-A82.
38 Y. M. Kang , M. S. Song , J. H. Kim , H. S. Kim , M. S. Park , J. Y. Lee and S. X. Dou, *Electrochim. Acta*, 2005, **50**, 3667-3673.
39 G. Binotto , D. Larcher , A. S. Prakash , R. Herrera Urbina , M. S. Hegde and J. M. Tarascon, *Chem. Mater.*, 2007, **19**, 3032-3040.
40 X. L. Wu , Y. G. Guo , L. J. Wan and C. W. Hu , *J. Phys. Chem. C*, 2008, **112**, 16824-16829.
41 H. Liu , G. X. Wang , J. Liu , S. Z. Qiao and H. Ahn , *J. Mater. Chem.*, 2011, **21**, 3046-3052.
42 X. Wang, H. Guan, S. M. Chen, H. Q. Li, T. Y. Zhai, D. M. Tang and Y. Bando, *Chem. Commun.*, 2011, **47**, 12280-12282.
43 J. Chen, X. H. Xia, J. P. Tu, Q. Q. Xiong, Y. X. Yu, X. L. Wang and C. D. Gu, *J. Mater. Chem.*, 2012, **22**, 15056–15061.
44 X. L. Chen, K. Gerasopoulos, J. C. Guo, A. Brown, C. S. Wang, R. Ghodssi and J. N. Culver, *ACS Nano*, 2010, **4**, 5366–5372.